Multiscale Theory in the Molecular Simulation of Electrolyte Solutions

ARTICLE *in* THE JOURNAL OF PHYSICAL CHEMISTRY B · JANUARY 2014

Impact Factor: 3.3 · DOI: 10.1021/jp410310m · Source: PubMed

3 AUTHORS:

Wei Zhang
Tulane University
5 PUBLICATIONS **1** CITATION
SEE PROFILE

Xinli You
Tulane University
10 PUBLICATIONS **10** CITATIONS
SEE PROFILE

Lawrence R. Pratt
Tulane University
203 PUBLICATIONS **9,202** CITATIONS
SEE PROFILE

THE JOURNAL OF PHYSICAL CHEMISTRY B

Article

pubs.acs.org/JPCB

Multiscale Theory in the Molecular Simulation of Electrolyte Solutions

W. Zhang, X. You, and L. R. Pratt*

Department of Chemical and Biomolecular Engineering, Tulane University, New Orleans, Lousiana 70118, United States

ABSTRACT: To define a role for AIMD simulation on the limited time and space scales accessible to those demanding methods, this paper organizes McMillan−Mayer theory, the potential distribution approach, and quasi-chemical theory to provide theory for the thermodynamic effects associated with long-length scales. The theory treats composition fluctuations that would be accessed by larger-scale calculations, and also longer-ranged interactions that are of special interest for electrolyte solutions. The quasi-chemical organization breaks-up governing free energies into physically distinct contributions: *packing*, *outer-shell*, and *chemical* contributions. Here we study specifically the *outer-shell* contributions that express electrolyte screening. For that purpose we adopt a primitive model suggested by observation of ion-pairing in tetraethylammonium tetrafluoroborate dissolved in propylene carbonate. Gaussian statistical models are shown to be effective physical models for *outer-shell* contributions, and they are conclusive for the free energies within the quasi-chemical formulation. With the present data set the Gaussian physical approximation obtains more accurate mean activity coefficients than does the Bennett direct evaluation of that free energy.

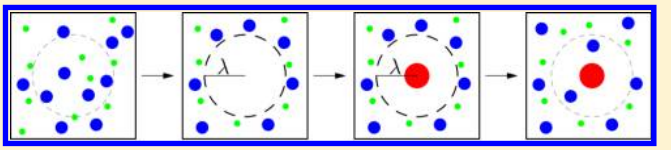

1. INTRODUCTION

This paper develops statistical mechanical theory with the goal of treating electrolyte solutions at chemical resolution. Our context is current research on electrochemical double-layer capacitors (EDLCs) based on nanotube forests.[1] The requirement of chemical resolution means that electronic structure must be an integral part of the theory consistent with the natural interest in chemical features of EDLCs.

Ab initio molecular dynamics (AIMD), though not statistical mechanical theory, is available to simulate electrolyte solutions. Compared to classic molecular simulations with empirical model force-fields, AIMD calculations are severely limited in space and time scales, by more than an order-of-magnitude in each. Consequently, application of AIMD is not feasible for EDLCs at scales that are experimentally interesting. This calls for further theory to embed AIMD methods in studies of EDCLs.

Change-of-scale consequences are a primitive goal of fundamental statistical mechanical theory. That basic perspective is explicit in the classic phase transition literature,[2] and it has long been relevant to the theory of electrolyte solutions specifically.[3,4] This paper organizes several basic results of the statistical mechanics of solutions to treat electrolyte solutions where space and time scales will otherwise prohibit direct AIMD calculations. Our results here suggest a role for AIMD somewhat analogous to subgrid modeling in computational fluid mechanics. Nevertheless, the goals of the statistical thermodynamics of complex solutions are distinct, and we do not propose transfer of results here between those fields.

Our development here utilizes several theoretical results that are "... both difficult and strongly established ..."[3] We put burdensome technical results in appendices, and in this introduction give a fuller discussion of the line of reasoning.

The initial step in our development is the McMillan−Mayer (MM) theory[3,5,6] *integrating out* of solvent degrees of freedom. MM theory is a pinnacle of coarse-graining for the statistical mechanics of solutions and achieves a vast conceptual simplification for the theory of electrolyte solutions. No sacrifice of molecular realism is implied by MM theory, and all primitive electrolyte solution models rest on it. But cataloging the multibody potentials required for a literal MM application is prohibitive.[7] Therefore, use of MM theory to construct a specific primitive model for a system of experimental interest has been limited.[8,9] Indeed, the MM theory is not generally suitable for specific molecular-scale implementation.

To address this, we exploit *quasi-chemical theory* (QCT), which is formally complete in its modern expression.[10,11] QCT evaluates solvation free energies by breaking them into contributions with clear physical meanings. One contribution is a *packing* contribution. This can be simple in the anticipated applications because the solvent is not involved specifically, and the ion concentrations are not prohibitively high. A second contribution (the *outer shell* contribution) treats ion−ion interactions at long-range and it is expected on physical grounds that the necessary MM interactions should be simple then. That outer-shell contribution is studied below.

The final contribution (the *chemical* contribution) treats ion−ion inner-shell neighbors. Smaller spatial scales must be directly confronted and it is here that the subgrid AIMD

Special Issue: James L. Skinner Festschrift

Received: October 17, 2013

dx.doi.org/10.1021/jp410310m | *J. Phys. Chem. B* XXXX, XXX, XXX−XXX

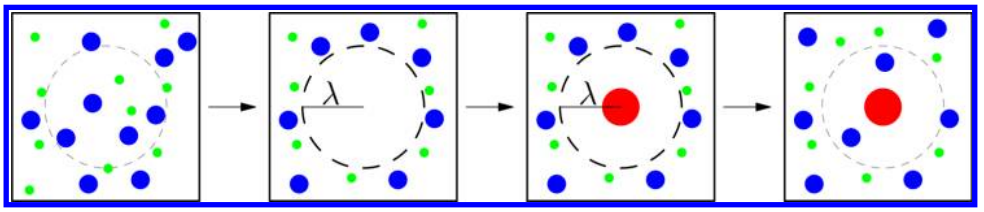

Figure 1. Evaluation of the excess chemical potential of a distinguished ion (red disk), patterned according to QCT. The blue and green disks are other ions in the system, and the solvent is in the background. The stepwise contributions are "packing", "outer shell", and "chemical" contributions, from left to right. See the text and eq 11 for further discussion.

activity comes into play. Figure 1 shows a now-standard picture of this organization of the statistical thermodynamical problem.

This discussion suggests that van der Waals theory is a subset of the present QCT approach. This is advantageous because van der Waals theory is the basis of the theory of liquids viewed broadly.[12,13] While paying an unavoidable price of significant computational effort, QCT goes beyond van der Waals theory in several ways. For example, here, where ion-pairing is an essential part of the physical picture, associative phenomena are treated fully. Furthermore, our QCT implementation would routinely treat outer-shell interactions through Gaussian order rather than the mean-field approach of classic van der Waals theories. This is essential in the present applications to capture the physical effect of Debye screening of ion correlations.

It is an interesting physical point that the identification of *packing* and *chemical* contributions here is a consequence of a choice of conditioning event, in the present development the emptiness of the inner-shell. This has the advantages that the theory is a close relative of van der Waals theory, and that the outer-shell contribution should be particularly simple to evaluate. But other choices of conditioning event are possible too.[14] For example, the conditioning event might be the event that the occupancy of the inner-shell is the value most probably observed. This has the intuitive attraction of being close to simple observations. But it presents the challenge that the evaluation of the partition function for that case might be more difficult. In what follows, our primary emphasis is to characterize the computational effort to evaluate the partition function associated with *outer-shell* contribution that arises with the original suggestion for the conditioning event.

The plan of this paper is as follows: Section 2 records several theoretical specifics that are required for our argument. Appendix A gives an accessible derivation of the MM theory results used here; Appendices B and C present technical features of the potential distribution theory and quasi-chemical theory, respectively, required in the main text. Section 3 gives a demonstration of the results obtained for a primitive electrolyte solution model that was designed to correspond to the tetraethylammonium tetrafluoroborate in propylene carbonate ([TEA][BF_4]/PC) where ion-pairing can be important.[15]

2. BASIC THEORY REQUIRED

2.1. McMillan–Mayer Theorem. The osmotic pressure, π, is evaluated as the partition function

$$e^{\beta\pi V} = \sum_{\mathbf{n}_A \geq 0} \mathcal{Z}(\mathbf{n}_A; z_S) \left(\frac{z_A^{\mathbf{n}_A}}{\mathbf{n}_A!} \right) \tag{1}$$

involving only the solute species A. Here V is the volume, $k_B T = \beta^{-1}$ is the temperature, and the activity of the solvent (species S) is denoted by $z_S = e^{\beta\mu_S}$. Equation 1 involves

$$\mathcal{Z}(\mathbf{n}_A; z_S) = \left[\lim_{z_A \to 0} \left(\frac{\rho_A}{z_A} \right)^{\mathbf{n}_A} \right] \int_V d1_A \ldots \int_V d\mathbf{n}_A \, e^{-\beta W(1_A \ldots \mathbf{n}_A)} \tag{2}$$

with ρ_A being the density of solutes, and with the potentials-of-average-force given by

$$W(1_A \ldots \mathbf{n}_A) = -\frac{1}{\beta} \ln g(1_A \ldots \mathbf{n}_A; z_S, z_A = 0) \tag{3}$$

which depends on the activity of the solvent. Equation 2 is compact, thermodynamically explicit, and general; see the Appendix for an accessible derivation and fuller discussion.

2.2. Potential Distribution Theorem (PDT). The solute chemical potential may be expressed as

$$\beta\mu_A = \ln \rho_A \Lambda_A{}^3 / q_A^{(\mathrm{int})} + \beta\mu_A^{(\mathrm{ex})}(z_A = 0) - \ln\langle\langle e^{-\beta\Delta W_A^{(1)}} \rangle\rangle_0 \tag{4}$$

The binding energy of a distinguished solute (A) molecule in the MM system is

$$\Delta W_A^{(1)} = W(\mathbf{n}_A + 1) - W(\mathbf{n}_A) - W(1) \tag{5}$$

The middle term of eq 4,

$$\beta\mu_A^{(\mathrm{ex})}(z_A = 0) = -\ln\langle\langle e^{-\beta\Delta U_A^{(1)}} \rangle\rangle_0 \tag{6}$$

is evaluated at infinite dilution of the solute. This evaluation is typically highly nontrivial, but much has been written about that[10,11] and we will proceed to analyze that right-most term of eq 4.

2.3. Quasi-Chemical Theory. Thus we study

$$\beta\Delta\mu_A^{(\mathrm{ex})} = \beta\mu_A^{(\mathrm{ex})} - \beta\mu_A^{(\mathrm{ex})}(z_A = 0) = -\ln\langle\langle e^{-\beta\Delta W_A^{(1)}} \rangle\rangle_0 \tag{7}$$

$\Delta\mu_A^{(\mathrm{ex})}$ is the contribution to the chemical potential of species A in excess of the infinite dilution result, due to interionic interactions with the influence of solvent fully considered.

A quasi-chemical development of eq 7 starts by characterizing neighborship. If the species considered are ions in solution, then we characterize ion neighbors of each ion in solution, distinguished in turn. Pairing of oppositely charged ions has been the subject of classic scientific history[15] that can inform the present discussion. Pairing of tetrafluoroborate 1-hexyl-3-methylimidazolium in pentanol has recently been studied both experimentally and computationally.[16]

Pairing of tetraethylammonium tetrafluoroborate in propylene carbonate is a helpful example.[15] In that case, pairing is simple to observe for saturated solution conditions and formation of chains and rings of ions is consistent with the molecular-scale observations. We might consider an indicator function χ_{AB} with the requirement that $\chi_{AB} = 1$ indicates *no* B ions are within an inner-shell stencil of a distinguished A ion. The simplest possibility, natural for compact molecular ions, is

dx.doi.org/10.1021/jp410310m | J. Phys. Chem. B XXXX, XXX, XXX–XXX

to identify a central atom in A and in B ions, and to set $\chi_{AB} = 1$ (but zero otherwise), when those atoms of further apart than a designated distance λ_{AB}.

Even simpler, and satisfactory for the primitive model that follows below, we might identify a central atom for ion A and then define a spherical inner-shell by the radius λ_A with the requirement that *no* other ions be closer than that. In fact, we choose the same radius for cations and anions in the primitive model studied below, $\lambda_A = \lambda_B = \lambda$.

Equation 7 was derived using the grand canonical ensemble. But implementation with simulations in the grand canonical ensemble would be painful. Calculations with *canonical* ensemble methods should be satisfactory. In what follows we will develop eq 7 from the perspective on the canonical ensemble. Appendix C discusses the relevant ensemble differences.

The canonical ensemble average of $e^{\beta\Delta W_A^{(1)}}\chi_A$ gives

$$\langle e^{\beta\Delta W_A^{(1)}}\chi_A\rangle = \frac{\langle\langle e^{-\beta\Delta W_A^{(1)}} e^{\beta\Delta W_A^{(1)}}\chi_A\rangle\rangle_0}{\langle\langle e^{-\beta\Delta W_A^{(1)}}\rangle\rangle_0} = e^{\beta\Delta\mu_A^{(ex)}}\langle\langle\chi_A\rangle\rangle_0 \tag{8}$$

In addition, for indicator function χ_A, and some other quantity G we have

$$\langle G\chi_A\rangle = \langle G|\chi_A = 1\rangle\langle\chi_A\rangle \tag{9}$$

Collecting these relations yields

$$e^{\beta\Delta\mu_A^{(ex)}} = \langle e^{\beta\Delta W_A^{(1)}}|\chi_A = 1\rangle\frac{\langle\chi_A\rangle}{\langle\langle\chi_A\rangle\rangle_0} \tag{10}$$

Evaluating the logarithm and replacing the conditional ensemble average with an integral over a conditional probability distribution, we get

$$\beta\Delta\mu_A^{(ex)} = -\ln\langle\langle\chi_A\rangle\rangle_0 + \ln\int e^{\beta\varepsilon}P_A(\varepsilon|\chi_A = 1)\,d\varepsilon + \ln\langle\chi_A\rangle \tag{11}$$

where

$$P_A(\varepsilon|\chi_A = 1) = \langle\delta(\varepsilon - \Delta W_A^{(1)})|\chi_A = 1\rangle \tag{12}$$

These three terms correspond to the three processes in Figure 1.

3. NUMERICAL DEMONSTRATION

We have tested how eq 11 works numerically on the basis of a primitive electrolyte solution model that was designed to correspond to the $[TEA][BF_4]$/PC. Table 1 describes the model further and indicates the thermodynamic states studied by Monte Carlo calculations. The radial distribution functions (Figure 2) show why this primitive model, with nonadditive hard-sphere interactions, was identified to study ion-pairing.

In this case, the packing and chemistry contributions can be directly calculated by trial insertions (for *packing* and $\langle\langle\chi_A\rangle\rangle_0$), and observation of the closest neighbor molecule distance distribution (for *chemistry* and $\langle\chi_A\rangle$). That leaves the *outer-shell* contribution which is our particular interest here.

For the general theory (eq 11 and Figure 1), the distinguished ion will be separated by a substantial distance from all other ions. We assume that the required MM binding energy can be approximated as a superposition of the pair potential-of-mean-force at long-range between the distinguished ion and all ion neighbors, which we take to be the classic macroscopic result $q_iq_j/4\pi\varepsilon r$ for a separation of r. That superposition is just the electrostatic interionic potential energy of interaction for the primitive model considered.

The system size correction of Hummer et al.[18] was applied to all binding energies, and thus to the free energies evaluated here.[19]

Table 1. Specifications for Monte Carlo Simulation of a Primitive Model with Dielectric Constant, Ion Charges, and Sizes Corresponding to the Atomically Detailed $[TEA][BF_4]$/PC Case[15a]

c (mol/dm^3)	L (nm)	$n_{\text{ion pairs}}$	κ^{-1} (nm)	$\beta q^2\kappa/2\varepsilon$
0.01	32.15	200	2.67	0.17
0.05	18.80	200	1.19	0.39
0.1	14.92	200	0.84	0.55
0.2	11.84	200	0.60	0.77
0.4	9.4	200	0.42	1.11
0.5	9.4	250	0.37	1.26
0.6	9.4	300	0.34	1.37
0.8	9.4	400	0.30	1.55
1.0	9.4	500	0.27	1.72
2.0	7.4	500	0.19	2.44

[a]Specifically, the model dielectric constant is $\varepsilon = 60$, and $d_{++} = 0.6668$ nm, $d_{--} = 0.6543$ nm, $d_{-+} = 0.45$ nm are distances of closest approach for the hard spherical ions. These calculations utilized the Towhee[17] package adapted to the present system, conventional cubical periodic boundary conditions at $T = 300$ K, and the indicated concentrations c. Each calculation was extended to 10^6 cycles after aging, each cycle comprising $2n_{\text{ion-pairs}}$ attempted moves. A total of 10 000 configurations are saved and used for the following analyses.

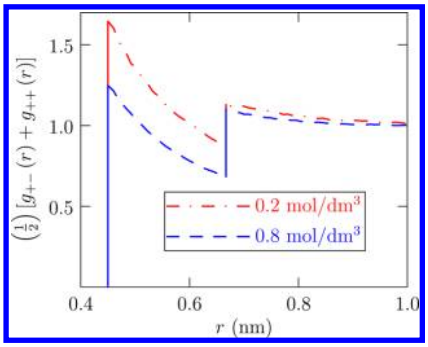

Figure 2. Radial distribution functions of $c = 0.2$ mol/dm^3 and $c = 0.8$ mol/dm^3 from cation to other ions. The two vertical lines identify the closest approach distances, which are 0.45 and 0.6668 nm in this case.

3.1. Binding Energy Distributions. We evaluate binding energies for the primitive model by standard Ewald calculation for configurations extracted from the Monte Carlo simulations, $\varepsilon = \Delta W_A^{(1)}$. We examine the distributions of binding energies for the ions present in the simulation, $P(\varepsilon)$, and also binding energies for permissible trial placements of additional anions or cations, $P^{(0)}(\varepsilon)$. For comparison, we do these calculations first *without* the conditioning prescribed by QCT, i.e., all anions or cations without regard to their neighborship status. Distributions of those binding energies (Figures 3–6) are striking. At the higher concentration shown (Figure 3), the distributions are reasonably normal as expected. At the lower concentration shown (Figure 4), the distributions are nongaussian. The design of the model to reflect ion-pairing is evident in the enhanced weight at substantially negative binding energies.

dx.doi.org/10.1021/jp410310m | J. Phys. Chem. B XXXX, XXX, XXX–XXX

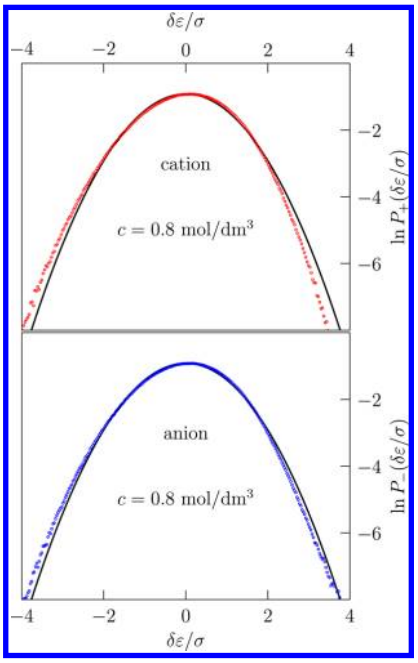

Figure 3. Observed distributions of ion binding energies, shifted and scaled into standard normal form, for c = 0.8 mol/dm^3. The parabolas (solid black lines) here are standard normal comparisons.

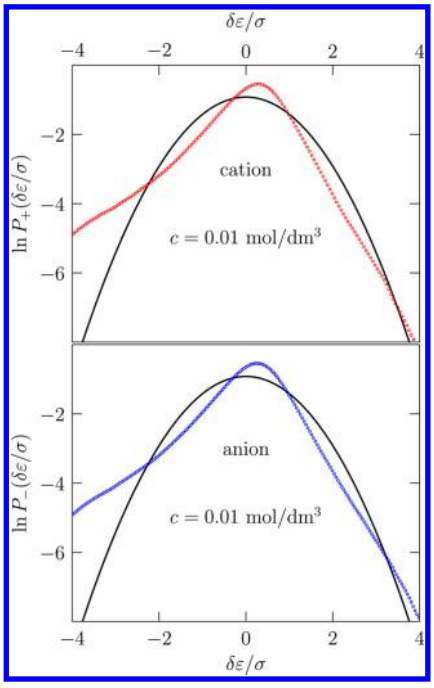

Figure 4. Observed distributions of ion binding energies, shifted and scaled into standard normal form, for c = 0.01 mol/dm^3. The parabolas (solid black lines) here are standard normal comparisons.

The normal presentation (as in Figures 3−7, shifted, scaled, and compared to standard normal) helps to judge the width of these distributions. An alternative presentation (Figures 8 and 9) compares these binding energy ranges to the thermal energy kT and gives additional insight. The free energy prediction from the coupled distributions (Figures 3 and 4) depends sensitively on the high-ε (right) wing of these graphs and hardly at all on the low-ε (left) wing. Even though the low-concentration distribution (Figure 4) is strikingly nongaussian, the right-wing

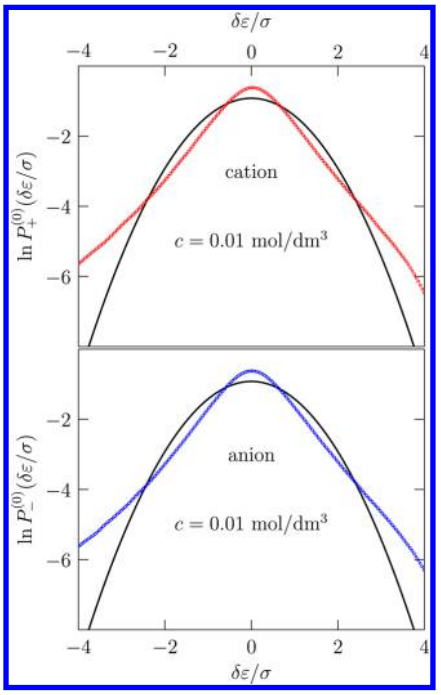

Figure 5. Observed distributions of uncoupled ion binding energies, shifted and scaled into standard normal form, for c = 0.01 mol/dm^3. The parabolas (solid black lines) here are standard normal comparisons.

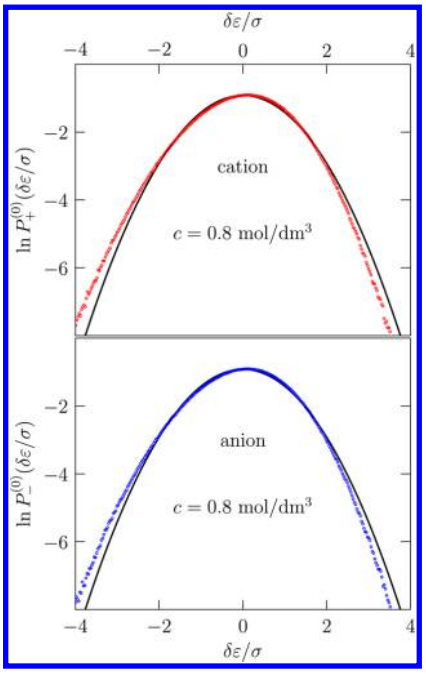

Figure 6. Observed distributions of uncoupled ion binding energies, shifted and scaled into standard normal form, for c = 0.8 mol/dm^3. The parabolas (solid black lines) here are standard normal comparisons.

extends, very roughly, to the same width as the natural Gaussian. In contrast, the uncoupled $P^{(0)}(\varepsilon)$ (Figure 5) is qualitatively nongaussian in both high-ε and low-ε wings.

The uncoupled $P^{(0)}(\varepsilon)$ (Figure 5) at low concentration is also distinctly abnormal, in both wings; at high-concentration they (Figure 6) are more nearly Gaussian.

dx.doi.org/10.1021/jp410310m | J. Phys. Chem. B XXXX, XXX, XXX−XXX

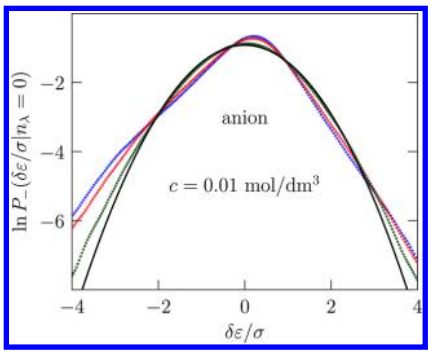

Figure 7. Probability density functions for the outer-shell binding energy for the anions in the simulation of Table 1, for the lowest concentration there, with λ = 0.7, 0.9, and 2.0 nm (blue, red, and green, respectively), compared with the standard normal (solid black curve). This demonstrates how increasing λ enforces better Gaussian behavior for this distribution.

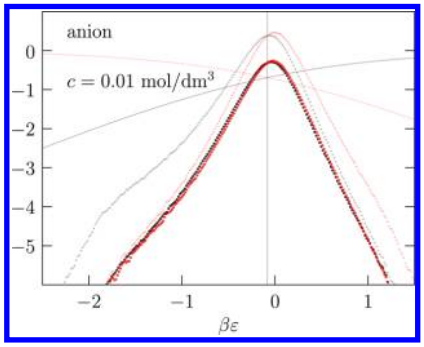

Figure 8. For the low concentration case of Table 1. The bold circles are the logarithms of the functions left and right of eq 15, black and red, respectively. The pale solid curves are the corresponding weight factors, e.g., $-\ln[1 + e^{\beta(\varepsilon-\Delta\mu_\alpha^{(ex)})}]$ for the red curve. The pale symbols are the plotted logarithms of the observed probability densities. The vertical line indicates the inferred value of the $\beta\Delta\mu_\alpha^{(ex)}$. Note that eq 15 is accurately satisfied.

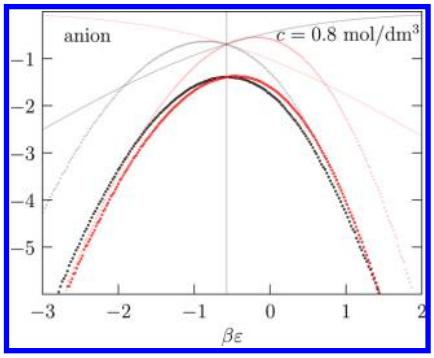

Figure 9. For the c = 0.8 mol/dm^3 case of Table 1. The bold circles are the logarithms of the functions left and right of eq 15, black and red, respectively. The pale solid curves are the corresponding weight factors, e.g., $-\ln[1 + e^{\beta(\varepsilon-\Delta\mu_\alpha^{(ex)})}]$ for the black curve. The pale symbols are the plotted logarithms of the observed probability densities. The vertical line shows the inferred value of the $\beta\Delta\mu^{(ex)}$. Note that eq 15 is only roughly satisfied in the low-ε wing.

3.2. QCT Conditioned Binding Energy Distributions.

We next consider the conditioned distributions that arise with the QCT approach (eq 11 and Figure 1). We take the inner-shell to be a sphere of radius λ centered on the ions. Typical results for $P_-(\delta\varepsilon/\sigma|n_\lambda = 0)$ for the interesting low concentration case (Figure 7) shows how the conditioning affects this distribution, with increasing λ driving the distribution toward normal behavior.

3.3. Free Energies and Gaussian Approximations.

The goal of our QCT development is to break the free energy into parts associated first with simple observations, and finally with a partition function calculation (the *outer-shell* contribution) that can be well approximated by a Gaussian model with simply observed parameters. In that case the *outer-shell* contribution of eq 11 would be

$$\ln \int e^{\beta\varepsilon} P_A(\varepsilon|\chi_A = 1)\, d\varepsilon \approx \beta\langle\varepsilon|\chi_A = 1\rangle + \beta^2\langle\delta\varepsilon^2|\chi_A = 1\rangle/2 \quad (13)$$

To test these ideas, we evaluate the free energies directly, with and without the QCT conditioning, and also compare the results of the Gaussian approximation eq 13.

The direct evaluation of the free energies follows Bennett's method,[20] and searches for the value $\Delta\mu^{(ex)}$ that solves

$$\left\langle \frac{1}{1 + e^{-\beta(\varepsilon-\Delta\mu_A^{(ex)})}} \right\rangle = \left\langle \frac{1}{1 + e^{\beta(\varepsilon-\Delta\mu_A^{(ex)})}} \right\rangle_0 \quad (14)$$

for each species considered. The average on the left is estimated with the sample associated with $P_A(\varepsilon)$ whereas the average on the right of uses the binding energies leading to $P_A^{(0)}(\varepsilon)$ associated with permissible trial placements.

3.3.1. No Conditioning. In this case, we estimate a nonelectrostatic contribution directly by trial insertions, then electrostatic contribution on the basis of distributions such as Figures 4 and 5. The mean activity coefficients (Figure 10) obtained with the Gaussian approximation and the Bennett evaluation are qualitatively similar but quantitatively different from each other.

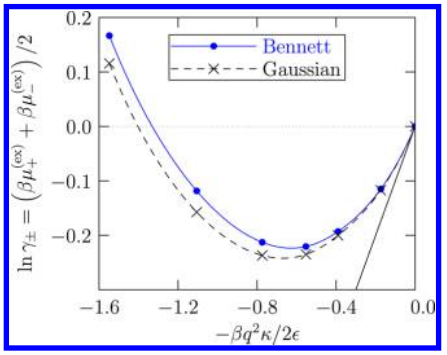

Figure 10. No conditioning, non-QCT, as discussed in section 3.3.1. The solid black line is the Debye–Hückel limiting law. The points correspond to c = {0.01, 0.05, 0.1, 0.2, 0.4, 0.8} mol/dm^3 cases of Table 1.

3.3.2. Pointwise Bennett Comparison. A more specific statement of the Bennett approach is

$$\frac{P(\varepsilon)}{1 + e^{-\beta(\varepsilon-\Delta\mu^{(ex)})}} = \frac{P^{(0)}(\varepsilon)}{1 + e^{\beta(\varepsilon-\Delta\mu^{(ex)})}} \quad (15)$$

This relies on the basic relation

$$P(\varepsilon) = e^{-\beta(\varepsilon-\Delta\mu^{(ex)})} P^{(0)}(\varepsilon) \quad (16)$$

and the elementary identity

dx.doi.org/10.1021/jp410310m | J. Phys. Chem. B XXXX, XXX, XXX–XXX

$$e^{-\beta(\varepsilon-\Delta\mu^{(ex)})} = \frac{1 + e^{-\beta(\varepsilon-\Delta\mu^{(ex)})}}{1 + e^{\beta(\varepsilon-\Delta\mu^{(ex)})}} \quad (17)$$

Equation 15 assembles information from $P(\varepsilon)$ and $P^{(0)}(\varepsilon)$ and thus illuminates the behavior of the important wings, high-ε for $P(\varepsilon)$ and low-ε for $P^{(0)}(\varepsilon)$. Typical results (Figures 8 and 9) show a reasonable match between the left and right side of eq 15. Note that at the higher concentration shown (Figure 9), the match in the low-probability wings is not perfect. A reasonable guess is that this is due to inaccuracy of $P^{(0)}(\varepsilon)$ at low-ε and that this is the reason behind the puzzling discrepancy between the Bennett result and the Gaussian model seen in Figures 10 and 13.

3.3.3. QCT Conditioning. Though the various QCT contributions depend on the radius λ of the inner-shell (Figure 11), the net free energy varies only slightly with increases of $\lambda >$

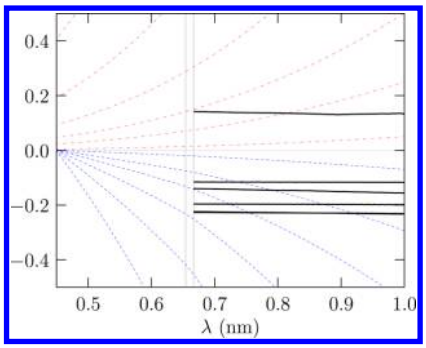

Figure 11. The red, blue, and black curves are the packing (arithmetic average of $-\ln\langle\langle\chi\rangle\rangle_0$ for the two ion types), chemical (arithmetic average of $\ln\langle\chi\rangle$ for the two ion types), and net contributions (following eq 11, including the outer-shell contribution, for $\ln\gamma_\pm$), respectively, for the primitive model results.[15] The various curves correspond to c = {0.01, 0.05, 0.1, 0.2, 0.4, 0.8} mol/dm^3 cases of Table 1.

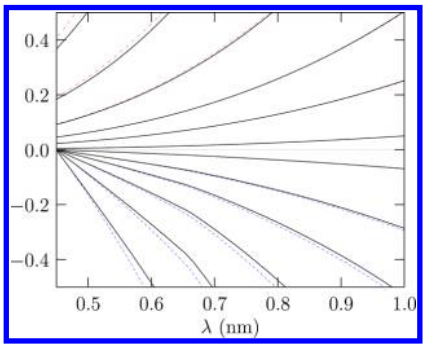

Figure 12. Upper black curves are the results from eq 18. Similarly, the red dot-dashed curves are the direct numerical results obtained by trail insertions. The lower black are the results from eq 19. Similarly, the blue dashed curves are the direct numerical results obtained by observations of the ions present in the simulations.

0.7 nm. The mean activity coefficients evaluated by the Bennett method and the Gaussian approximation (Figure 13) now accurately agree. This suggests that both approaches are physically reliable with this conditioning. For the MM pair-potential at long-range to be plausibly exploited, the conditioning is essential to the broader idea here.

For the concentrations and λ values in Figure 11, the Poisson estimates of the packing and chemical contributions[15]

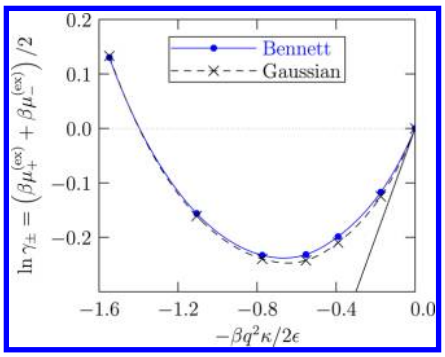

Figure 13. QCT, as discussed in section 3.3.3. The solid black line is the Debye−Hückel limiting law.

$$-\ln\langle\langle\chi\rangle\rangle_0 \equiv -\sum_\alpha \ln\langle\langle\chi_\alpha\rangle\rangle_0 = \left(\frac{1}{2}\right)\sum_{\alpha,\gamma}\frac{4\pi}{3}\lambda^3 c \quad (18)$$

$$-\ln\langle\chi\rangle \equiv -\sum_\alpha \ln\langle\chi_\alpha\rangle = \left(\frac{1}{2}\right)\sum_{\alpha,\gamma} 4\pi\int_0^\lambda c g_{\alpha\gamma}(r) r^2\, dr \quad (19)$$

are useful. The combination

$$-\ln\left[\frac{\langle\langle\chi\rangle\rangle_0}{\langle\chi\rangle}\right] = -\left(\frac{1}{2}\right)\sum_{\alpha,\gamma} 4\pi\int_0^\lambda c[g_{\alpha\gamma}(r) - 1] r^2\, dr \quad (20)$$

is then interesting. The utility of these results emphasize again that the ion densities are not high, so simple results can be helpful.

4. CONCLUSIONS

This paper organizes several basic theoretical results (McMillan−Mayer theory, the potential distribution approach, and quasi-chemical theory) to apply high-resolution AIMD to electrolyte solutions. The conceptual target for these considerations is that the last of the calculations depicted in Figure 1 can be done by AIMD directly on the time and space scales typical of those demanding methods. This theory then develops a mechanism for addressing effects associated with longer spatial scales, involving also characteristically longer time scales. The theory treats composition fluctuations which would be accessed by larger-scale calculations, and also longer-ranged interactions and correlations that are of special interest for electrolyte solutions.

The quasi-chemical organization, as an extension of van der Waals pictures, breaks-up governing free energies into physically distinct contributions: *packing*, *outer-shell*, and *chemical* contributions. This paper adopted a primitive model suggested by observed ion-pairing in tetraethylammonium tetrafluoroborate dissolved in propylene carbonate and then studied specifically the *outer-shell* contributions that expresses electrolyte screening. Gaussian statistical models are shown to be effective as physical models for these *outer-shell* contributions, and they are conclusive for the free energies within the quasi-chemical formulation (Figures 11 and 13). In fact, with this data set the Gaussian physical approximation is more efficient in providing an accurate mean activity coefficient than is the Bennett direct evaluation of that free energy (Figures 10 and 13).

dx.doi.org/10.1021/jp410310m | J. Phys. Chem. B XXXX, XXX, XXX−XXX

APPENDIX A: ACCESSIBLE DERIVATION OF THE MCMILLAN–MAYER THEORY

In the analysis of the MM theory, the formulas that are employed can be intimidating[21−23] at several stages so a physically clear notation helps. We consider a system composed of solvent (S) and solutes (A). The numbers of these species will be indicated by $\mathbf{n}_S$ and $\mathbf{n}_A$, the boldface typography indicating that each of these quantities can be multicomponent, i.e., $\mathbf{n}_A = \{n_{A1}, n_{A2}, ...\}$, and similarly for solvent species. The Helmholtz free energy $A(T,V,\mathbf{n}_S,\mathbf{n}_A)$ then leads to the canonical partition function

$$e^{-\beta A(T,V,\mathbf{n}_S,\mathbf{n}_A)} = Q(\mathbf{n}_S,\mathbf{n}_A)/(\mathbf{n}_S!\mathbf{n}_A!) \tag{A-1}$$

T (temperature) and V (volume) have their usual meanings, and we will suppress that notation on the right of eq A-1. To further fix the notation, we recall[19] $Q(\mathbf{n}_A = 1) \equiv Vq_A^{(int)}/\Lambda_A{}^3$ is the canonical ensemble partition function for a system comprising exactly one molecule of type A in a volume V with Λ_A is the thermal de Broglie wavelength. The factorial notation

$$\mathbf{n}_A! = n_{A_1}!n_{A_2}!\cdots \tag{A-2}$$

is common.[19,21] When convenient, we will denote $n = \{\mathbf{n}_S, \mathbf{n}_A\}$ so that

$$e^{-\beta A(T,V,n)} = Q(n)/n! \tag{A-3}$$

The grand canonical partition function will be central,

$$e^{\beta pV} = \sum_{n\geq 0} Q(n)\left(\frac{z^n}{n!}\right) \tag{A-4}$$

in these terms. Here we adopt a correspondingly simplified notation for the activities[19,21]

$$z^n = \exp\{\sum_X \beta\mu_X n_X\} \tag{A-5}$$

with μ_X the chemical potential of species X. We will compare the pressure of the solution with the pressure of the solvent-only system at the same activity $z_S = e^{\beta\mu_S}$:

$$e^{\beta(p-\pi)V} = \sum_{\mathbf{n}_S\geq 0} Q(\mathbf{n}_S,\mathbf{n}_A=0)\left(\frac{z_S{}^{\mathbf{n}_S}}{\mathbf{n}_S!}\right) \tag{A-6}$$

The pressure difference π is the osmotic pressure. The probability for observing $\mathbf{n}_S$ in the solvent-only system is

$$P(\mathbf{n}_S;z_A=0) = Q(\mathbf{n}_S,\mathbf{n}_A=0)\left(\frac{z_S{}^{\mathbf{n}_S}}{\mathbf{n}_S!}\right)e^{-\beta(p-\pi)V} \tag{A-7}$$

With these notations we write

$$e^{\beta\pi V}\sum_{\mathbf{n}_A\geq 0}\left(\frac{z_A{}^{\mathbf{n}_A}}{\mathbf{n}_A!}\right)\sum_{\mathbf{n}_S\geq 0}\left\{\frac{Q(\mathbf{n}_S,\mathbf{n}_A)}{Q(\mathbf{n}_S,\mathbf{n}_A=0)}\right\}P(\mathbf{n}_S;z_A=0)$$
$$= \sum_{\mathbf{n}_A\geq 0}\mathcal{Z}(\mathbf{n}_A;z_S)\left(\frac{z_A{}^{\mathbf{n}_A}}{\mathbf{n}_A!}\right) \tag{A-8}$$

The important point is the structural similarity to eq A-4.

Our task is to analyze the MM configurational integral

$$\mathcal{Z}(\mathbf{n}_A;z_S) = \sum_{\mathbf{n}_S\geq 0}\left\{\frac{Q(\mathbf{n}_S,\mathbf{n}_A)}{Q(\mathbf{n}_S,\mathbf{n}_A=0)}\right\}P(\mathbf{n}_S;z_A=0) \tag{A-9}$$

The displayed ratio of partition functions is distinctive. For the case $\mathbf{n}_A = 1$, for example, we write

$$\sum_{\mathbf{n}_S\geq 0}\left\{\frac{Q(\mathbf{n}_S,\mathbf{n}_A=1)}{Q(\mathbf{n}_S,\mathbf{n}_A=0)}\right\}P(\mathbf{n}_S;z_A=0)$$
$$= Q(\mathbf{n}_s=0,\mathbf{n}_A=1)\langle\langle e^{-\beta\Delta U_A^{(1)}}\rangle\rangle_0 \tag{A-10}$$

where the right-most factor is to be evaluated at infinite dilution of the solute, $z_A = 0$. The potential distribution development establishes that right side to be[19]

$$Q(\mathbf{n}_S=0,\mathbf{n}_A=1)\langle\langle e^{-\beta\Delta U_A^{(1)}}\rangle\rangle_0 = \lim_{z_A\to 0}\left(\frac{\mathbf{n}_A}{z_A}\right) = \lim_{z_A\to 0}\left(\frac{\rho_A}{z_A}\right)V \tag{A-11}$$

To write the general term for eq A-9, we will use

$$\binom{\mathbf{n}_A}{\mathbf{m}_A}$$

to denote the number of ways of selecting the $\mathbf{m}_A$ solute molecule set from the collection $\mathbf{n}_A$. For example, if only one type of solute A is considered, then

$$\binom{\mathbf{n}_A}{\mathbf{m}_A} = \frac{\mathbf{n}_A!}{\mathbf{m}_A!(\mathbf{n}_A-\mathbf{m}_A)!} = \frac{\mathbf{n}_A^{\underline{\mathbf{m}_A}}}{\mathbf{m}_A!} \tag{A-12}$$

as usual, with the last equality using the "$\mathbf{n}_A$-to-the-$\mathbf{m}_A$-falling" notation.[19,24]

For more general but specified $\mathbf{m}_A$, we rewrite eq A-9

$$\sum_{\mathbf{n}_S\geq 0}\left\{\frac{Q(\mathbf{n}_S,\mathbf{m}_A)}{Q(\mathbf{n}_S,\mathbf{m}_A=0)}\right\}P(\mathbf{n}_S;z_A=0)$$
$$= Q(\mathbf{n}_S=0,\mathbf{m}_A)\langle\langle e^{-\beta\Delta U^{(\mathbf{m}_A)}}\rangle\rangle_0 \tag{A-13}$$

and again, after having set $\mathbf{m}_A$, this is to be evaluated at infinite dilution. Here the binding energy

$$\Delta U^{(\mathbf{m}_A)} = U(\mathbf{n}_S,\mathbf{m}_A) - U(\mathbf{n}_S,\mathbf{m}_A=0) - U(\mathbf{n}_S=0,\mathbf{m}_A) \tag{A-14}$$

is associated with the collection of $\mathbf{m}_A$ solute molecules. Following the potential distribution theory further[19]

$$Q(\mathbf{n}_S=0,\mathbf{m}_A)\langle\langle e^{-\beta\Delta U^{(\mathbf{m}_A)}}\rangle\rangle_0 = \left\langle\binom{\mathbf{n}_A}{m_A}\right\rangle\frac{\mathbf{m}_A!}{z_A{}^{\mathbf{m}_A}} \tag{A-15}$$

Finally,

$$\left\langle\binom{\mathbf{n}_A}{\mathbf{m}_A}\right\rangle\mathbf{m}_A! = \rho_A{}^{\mathbf{m}_A}\int_V d1_A\ldots\int_V d\mathbf{m}_A\, g^{(\mathbf{m}_A)}(1_A\ldots\mathbf{m}_A) \tag{A-16}$$

with $g^{(\mathbf{m}_A)}(1_A\ldots\mathbf{m}_A)$ denoting the usual $\mathbf{m}_A$ joint distribution function. Here we denote solute configurational coordinates as $(1_A\ldots\mathbf{m}_A)$, and the necessary integrations by $\int_V d1_A\ldots\int_V d\mathbf{m}_A$. This produces the factor of V in eq A-11. Because we wish to simplify eq A-13, with $z_A = 0$, we use eq A-15 to write

$$\mathcal{Z}(\mathbf{n}_A;z_S)$$
$$= \lim_{z_A\to 0}\left(\frac{\rho_A}{z_A}\right)^{\mathbf{n}_A}\int_V d1_A\ldots\int_V d\mathbf{n}_A g^{(n_A)}(1_A\ldots\mathbf{n}_A;z_A=0) \tag{A-17}$$

The prefactor, to be evaluated at infinite dilution, is given by

dx.doi.org/10.1021/jp410310m | J. Phys. Chem. B XXXX, XXX, XXX−XXX

$$\frac{\rho_A}{z_A} = \frac{q_A^{int}}{{\Lambda_A}^3}\langle\langle e^{-\beta\Delta U_A^{(1)}}\rangle\rangle_0 \tag{A-18}$$

in the potential distribution theorem formulation.[19]

With this suggestive form we can be more specific about the canonical configurational integrals that started our discussion, specifically

$$\begin{aligned} Q(\mathbf{n}_A) &= \lim_{z_S\to 0} \mathcal{Z}(\mathbf{n}_A;z_S) \\ &= \lim_{z_S\to 0}\left[\lim_{z_A\to 0}\left(\frac{\rho_A}{z_A}\right)\right]^{\mathbf{n}_A}\int_V d1_A \ldots \int_V d\mathbf{n}_A\, e^{-\beta W(1_A\ldots\mathbf{n}_A)} \end{aligned} \tag{A-19}$$

The multipliers supply features of the kinetic energy portion of the partition function, specific to the implementation for the particular case. For notational simplicity we will drop the specific identification of the solvent activity in the formulas elsewhere.

These formulas, particularly eq A-19, are collected in the summary statement of MM theory in section 2.1, and particularly with eq 2.

APPENDIX B: POTENTIAL DISTRIBUTION THEORY

With the MM background, we evaluate the average number of solute A molecules as

$$\langle\mathbf{n}_A\rangle = e^{-\beta\pi V}\sum_{\mathbf{n}_A\geq 0}\mathbf{n}_A\mathcal{Z}(\mathbf{n}_A;z_S)\left(\frac{{z_A}^{\mathbf{n}_A}}{\mathbf{n}_A!}\right) \tag{B-1}$$

Because the summand factor $\mathbf{n}_A$ annuls the $\mathbf{n}_A = 0$ term, this result presents an explicit leading factor of z_A. Determination of z_A establishes the thermodynamic property μ_A. Therefore, we rewrite this equation by bringing forward the explicit extra factor of z_A as

$$\begin{aligned} \langle\mathbf{n}_A\rangle = e^{-\beta\pi V}\mathcal{Z}(\mathbf{n}_A{=}1;z_S)z_A \times \\ \sum_{\mathbf{n}_A\geq 0}\left(\frac{\mathcal{Z}(\mathbf{n}_A{+}1;z_S)}{\mathcal{Z}(\mathbf{n}_A{=}1;z_S)\mathcal{Z}(\mathbf{n}_A;z_S)}\right)\mathcal{Z}(\mathbf{n}_A;z_S)\left(\frac{{z_A}^{\mathbf{n}_A}}{\mathbf{n}_A!}\right) \end{aligned} \tag{B-2}$$

or

$$\langle\mathbf{n}_A\rangle = \mathcal{Z}(\mathbf{n}_A{=}1;z_S)z_A\langle\langle e^{-\beta\Delta W_A^{(1)}}\rangle\rangle_0 \tag{B-3}$$

Here

$$\Delta W_A^{(1)} = W(\mathbf{n}_A + 1) - W(\mathbf{n}_A) - W(1) \tag{B-4}$$

is the binding energy of a distinguished solute (A) molecule in the MM system, and the quantity

$$\mathcal{Z}(\mathbf{n}_A{=}1;z_S) = \frac{Vq_A^{(int)}}{{\Lambda_A}^3}\langle\langle e^{-\beta\Delta U_A^{(1)}}\rangle\rangle_0 \tag{B-5}$$

involves interactions of one A molecule and the solvent; it is proportional to the system volume.

APPENDIX C: QCT BREAKUP IN THE GRAND CANONICAL ENSEMBLE

Here we discuss twists associated with the consideration of PDT developments when $\mathbf{n}_A$ fluctuates. We begin with the observation from eq B-3 that

$$\langle\langle e^{-\beta\Delta W_A^{(1)}}\rangle\rangle_0 \propto \langle\mathbf{n}_A\rangle \tag{C-1}$$

Then considering the ratio

$$\frac{\langle\langle e^{-\beta\Delta W_A^{(1)}}F\rangle\rangle_0}{\langle\langle e^{-\beta\Delta W_A^{(1)}}\rangle\rangle_0} = \frac{\langle F\mathbf{n}_A\rangle}{\langle n\mathbf{n}_A\rangle} \tag{C-2}$$

yields a particularly transparent result. Choosing $F = e^{\beta\Delta W_A^{(1)}}\chi_A$, we obtain an analogue of eq 8:

$$\frac{\langle e^{\beta\Delta W_A^{(1)}}\chi_A\mathbf{n}_A\rangle}{\langle\mathbf{n}_A\rangle} = \frac{\langle\langle\chi_A\rangle\rangle_0}{\langle\langle e^{-\beta\Delta W_A^{(1)}}\rangle\rangle_0} \tag{C-3}$$

If the averages are canonical, then this is just eq 8 again, but eq C-3 remains true if $\mathbf{n}_A$ fluctuates.

We expect that

$$\frac{\langle e^{\beta\Delta W_A^{(1)}}\chi_A\mathbf{n}_A\rangle}{\langle\mathbf{n}_A\rangle} \sim \langle e^{\beta\Delta W_A^{(1)}}\chi_A\rangle + O(\langle\mathbf{n}_A\rangle^{-1}) \tag{C-4}$$

so in the thermodynamic limit that average matches the simpler canonical expression. The reason for this expectation is that we can write $\mathbf{n}_A = \langle\mathbf{n}_A\rangle + \delta\mathbf{n}_A$ in the numerator. Then the correlation of $\delta\mathbf{n}_A$ with the intensive characteristic of that numerator average should yield an intensive result.

Accepting this argument for the moment and retaining only the dominant contribution in eq C-4, we recover the results of section 2.3, and specifically the important result eq 11, but consistently with the grand canonical ensemble derivation of the earlier sections.

To make that physical view specific, we introduce the additional notation

$$\langle e^{\beta\Delta W_A^{(1)}}|\mathbf{n}_A\rangle$$

for the canonical ensemble average that specifies $\mathbf{n}_A$. For anticipated $\delta\mathbf{n}_A$, we use

$$\begin{aligned} \langle e^{\beta\Delta W^{(1)}}\chi_A|\mathbf{n}_A\rangle \approx \langle e^{\beta\Delta W_A^{(1)}}\chi_A|\langle\mathbf{n}_A\rangle\rangle \\ + \delta\mathbf{n}_A\left(\frac{\partial\langle e^{\beta\Delta W_A^{(1)}}\chi_A|\langle\mathbf{n}_A\rangle\rangle}{\partial\langle\mathbf{n}_A\rangle}\right) \end{aligned} \tag{C-5}$$

Using this in the left side of eq C-4 and then averaging with respect to $\mathbf{n}_A$ occupancies yield

$$\begin{aligned} \frac{\langle e^{\beta\Delta W_A^{(1)}}\chi_A\mathbf{n}_A\rangle}{\langle\mathbf{n}_A\rangle} \approx \langle e^{\beta\Delta W_A^{(1)}}\chi_A|\langle\mathbf{n}_A\rangle\rangle \\ + \frac{\langle\delta{\mathbf{n}_A}^2\rangle}{\langle\mathbf{n}_A\rangle}\left(\frac{\partial\langle e^{\beta\Delta W_A^{(1)}}\chi_A|\langle\mathbf{n}_A\rangle\rangle}{\partial\langle\mathbf{n}_A\rangle}\right) \end{aligned} \tag{C-6}$$

the expected result. Because

$$\langle\delta{\mathbf{n}_A}^2\rangle = \left(\frac{\partial\langle\mathbf{n}_A\rangle}{\partial\beta\mu_A}\right)_{T,V,\mu_S}$$

the correction indeed vanishes in the thermodynamic limit.

dx.doi.org/10.1021/jp410310m | J. Phys. Chem. B XXXX, XXX, XXX−XXX

AUTHOR INFORMATION

Corresponding Author

*L. R. Pratt: e-mail, lpratt@tulane.edu; phone, +1 504 862 8929; fax: +1 504 865 6744.

Notes

The authors declare no competing financial interest.

ACKNOWLEDGMENTS

This work was supported by the National Science Foundation under the NSF EPSCoR Cooperative Agreement No. EPS-1003897, with additional support from the Louisiana Board of Regents.

REFERENCES

(1) Yang, L.; Fishbine, B. H.; Migliori, A.; Pratt, L. R. Dielectric Saturation of Liquid Propylene Carbonate in Electrical Energy Storage Applications. *J. Chem. Phys.* **2010**, *132*, 044701(1−4).
(2) Ma, S. K. *Modern Theory of Critical Phenomena*; W. A. Benjamin, Inc: Reading, MA, 1976.
(3) Friedman, H. L.; Dale, W. D. T. In *Statistical Mechanics Part A: Equilibrium Techniques*; Berne, B. J., Ed.; Plenum: New York, 1977; pp 85−136.
(4) Friedman, H. L. Electrolyte Solutions at Equilibrium. *Annu. Rev. Phys. Chem.* **1981**, *32*, 1798−204.
(5) McMillan, W. G., Jr.; Mayer, J. E. The Statistical Thermodynamics of Multicomponent Systems. *J. Chem. Phys.* **1945**, *13*, 276−305.
(6) Hill, T. L. *Statistical Thermodynamics*; Addison-Wesley: Reading, MA, 1960; Chapter SS19.1.
(7) Adelman, S. A. The Effective Direct Correlation Function, an Approach to the Theory of Liquids Solutions: A New Definition of the Effective Solute Potential. *Chem. Phys. Lett.* **1976**, *38*, 567−570.
(8) Kusalik, P. G.; Patey, G. N. On the Molecular Theory of Aqueous Electrolyte Solutions. III. A Comparison between Born-Oppenheimer and McMillan-Mayer Levels of Description. *J. Chem. Phys.* **1988**, *89*, 7478−7484.
(9) Ursenbach, C. P.; Wei, D.; Patey, G. N. Activity Coefficient of Model Aqueous Electrolyte Solutions: Sensitivity to the Short Range Part of the Interionic Potential. *J. Chem. Phys.* **1991**, *94*, 6782−6784.
(10) Asthagiri, D.; Dixit, P. D.; Merchant, S.; Paulaitis, M. E.; Pratt, L. R.; Rempe, S. B.; Varma, S. Ion Selectivity from Local Configurations of Ligands in Solutions and Ion Channels. *Chem. Phys. Lett.* **2010**, *485*, 1−7.
(11) Sabo, D.; Jiao, D.; Varma, S.; Pratt, L. R.; Rempe, S. B. Case Study of Rb+(aq), Quasi-chemical Theory of Ion Hydration, and the No Split Occupancies Rule. *Annu. Rep. Prog. Chem. Soc. C* **2013**, *109*, 266−278.
(12) Widom, B. Intermolecular Forces and the Nature of the Liquid State. *Science* **1967**, *157*, 375−382.
(13) Chandler, D.; Weeks, J. D.; Andersen, H. C. van der Waals Picture of Liquids, Solids, and Phase Transitions. *Science* **1983**, *220*, 787−794.
(14) Rogers, D. M.; Jiao, D.; Pratt, L. R.; Rempe, S. B. Structural Models and Molecular Thermodynamics of Hydration of Ions and Small Molecules. *Annu. Rep. Comput. Chem.* **2012**, *8*, 71−127.
(15) Zhu, P.; You, X.; Pratt, L. R.; Papadopoulos, K. D. Generalizations of the Fuoss Approximation for Ion Pairing. *J. Chem. Phys.* **2011**, *134*, 054502.
(16) Zhu, P.; Pratt, L. R.; Papadopoulos, K. D. Pairing of 1-Hexyl-3-methylimidazolium and Tetrafluoroborate Ions in n-Pentanol. *J. Chem. Phys.* **2012**, *137*, 174501.
(17) Martin, M. G. *Towhee*, 2010; http://sourceforge.net/projects/towhee/.
(18) Hummer, G.; Pratt, L. R.; García, A. E. Free Energy of Ionic Hydration. *J. Phys. Chem.* **1996**, *100*, 1206−1215.
(19) Beck, T. L.; Paulaitis, M. E.; Pratt, L. R. *The Potential Distribution Theorem and Models of Molecular Solutions*; Cambridge University Press: Oxford, U.K., 2006.
(20) Bennett, C. H. Efficient Estimation of Free Energy Differences from Monte Carlo Data. *J. Comput. Phys.* **1976**, *22*, 245−268.
(21) Mayer, J. E.; Mayer, M. G. *Statistical Mechanics*, 2nd ed.; Wiley-Interscience: New York, 1977.
(22) Münster, A. *Statistical Thermodynamics*; Academic Press, New York, 1974; Vol. 2.
(23) Friedman, H. L. *Ionic Solution Theory*; Interscience: New York, 1962.
(24) Graham, R. L.; Knuth, D. E.; Patashnik, O. *Concrete Mathematics*; Addison-Wesley: Reading, MA, 1989.